Simulation and inversion of ultrasonic pitch-catch through-tubing well logging with an array of receivers

Erlend Magnus Viggen[a,*], Tonni Franke Johansen[a], Ioan-Alexandru Merciu[b]

[a]*Department of acoustics, SINTEF ICT, Strindvegen 4, Trondheim, Norway*
[b]*Statoil ASA, Research, Development, and Innovation, MADI DWS WI, Arkitekt Ebbells veg 10, Rotvoll, Norway*

Abstract

Current methods for ultrasonic pitch-catch well logging use two receivers to log the bonded material outside a single casing. For two casings separated by a fluid, we find by simulation that increasing the number of receivers provides a better picture of the effect of the bonded material outside the second casing. Inverting simulated measurements with five receivers, using a simulated annealing algorithm and a simple forward model, we find for a subset of simulations that we can estimate the impedance of the material outside the second casing.

Keywords: well logging, ultrasonic pitch-catch measurement, finite element simulation, mathematical modelling, inversion

1. Introduction

Multiple-casing well logging is a topic of increasing importance, in particular due to the large number of upcoming plug & abandonment operations [1]. Though very little has been published so far on ultrasonic logging in multiple-casing wells [1], ultrasonic logging in single-casing wells has been extensively studied [2, 3, 4, 5]. Current methods for single-casing pitch-catch well logging use two receivers, as this is sufficient to measure the exponential attenuation of the primary Lamb wave packet on the inner casing. This attenuation can be used to determine the impedance of the bonded material outside the casing [3, 4].

In a double-casing geometry as shown in Figure 1, it has been found [1] that there appears a cascade of leaky Lamb wave packets between the two casings where later packets feed on earlier ones. The amplitudes of the wave packets and their emitted wavefronts are proportional. By

*Corresponding author
Email address: erlendmagnus.viggen@sintef.no (Erlend Magnus Viggen)

Table 1: P-wave speed c_p, density ρ, impedance Z, and s-wave speed c_s of simulated materials.

Material	c_p [m/s]	ρ [kg/m^3]	Z [MRayl]	c_s [m/s]
Scree	300	1700	0.51	0
Water	1481	1000	1.48	0
Sat. shales & clays	1200	2050	2.46	0
Foam cement	2250	1330	2.99	767
Sat. shales & sand sect.	1750	2150	3.76	336
Chalk	2400	1900	4.56	897
Marls	2400	2200	5.28	897
Poro. & sat. sandstn.	2600	2300	5.98	1069
Class G cement	3700	1800	6.66	2017
Formation	4645	2200	10.2	2646
Steel casing	5780	7850	45.4	3190

measuring a wavefront's amplitude, the pitch-catch receivers R_i can thus indirectly measure the relative amplitude of the corresponding wave packet at the time when it emitted the measured part on the wavefront. It has been found [1] that the wave packet amplitudes evolve according to the system geometry and material parameters such as the impedance Z_B of the bonded material in the B-annulus, and that this impedance affects the amplitudes measured by the receivers from later wavefronts.

From these considerations we believe that increasing the number of receivers will improve the possibility and accuracy of inversion to determine the system's parameters, as more points along the packets' evolution are then measured. In this letter we show and discuss results of finite element simulations with five receivers, and demonstrate the possibility of inversion in a subset of the simulated cases.

2. Simulation setup

Finite element simulations were performed in the system's two-dimensional cross-section. The simulation setup, shown in Figure 1, is identical to that in [1], with the exception that five receivers

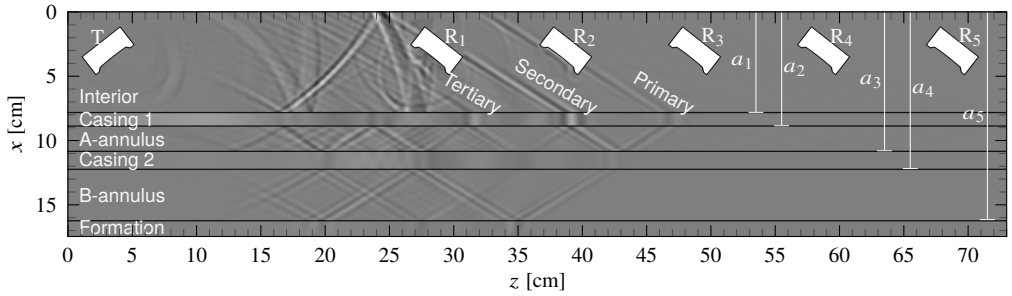

Figure 1: Snapshot of the simulated system at 170 µs with water in all annuli, showing pressure in the fluids and x-displacement in the solids

are used instead of two. The receivers R_i are positioned 10 cm apart. The first receiver's face centre is 25 cm away from the transmitter's face centre. The inner casing has a diameter $2a_2 = 7$ in and a thickness $a_2 - a_1 = 0.408$ in, while the outer has a diameter $2a_4 = 9\frac{5}{8}$ in and a thickness $a_4 - a_3 = 0.545$ in.

We restrict ourselves to a simple through-tubing case with water in the interior and the A-annulus, and a variety of materials given in Table 1 in the B-annulus. An empirical relation [6] was used for the s-wave speed c_s of materials where this parameter was unknown, and materials where this relation would give $c_\mathrm{s} < 0$ were treated as fluids ($c_\mathrm{s} = 0$).

3. Simulation results and discussion

The simulation snapshot in Figure 1 shows the train of wave packets on both casings, and the leaky wavefronts connecting these. The wavefronts emitted by the packets on the inner casing are measured by the receivers, which filter the impinging pressures and return nondimensionalised signals $S_{\mathrm{R}_i}(t)$. As a wavefront's amplitude is proportional to its wave packet's amplitude at the time of emission, the received wavefront signals shown in Figure 2a tell of the wave packets' evolution. The peak amplitude corresponding to wavefront k in the envelope of $S_{\mathrm{R}_i}(t)$ is denoted as $S_{\mathrm{R}_i,k}$.

In Figure 2a we see that the primary wavefront decreases exponentially, the secondary wavefront peaks between R_1 and R_2, and the tertiary wavefront experiences a polarity change [1] between R_3 and R_4 where its magnitude reaches zero and starts increasing again. With only two receivers, this information could not have been captured.

The evolution of the first few wavefronts for various B-annulus materials is shown in for the

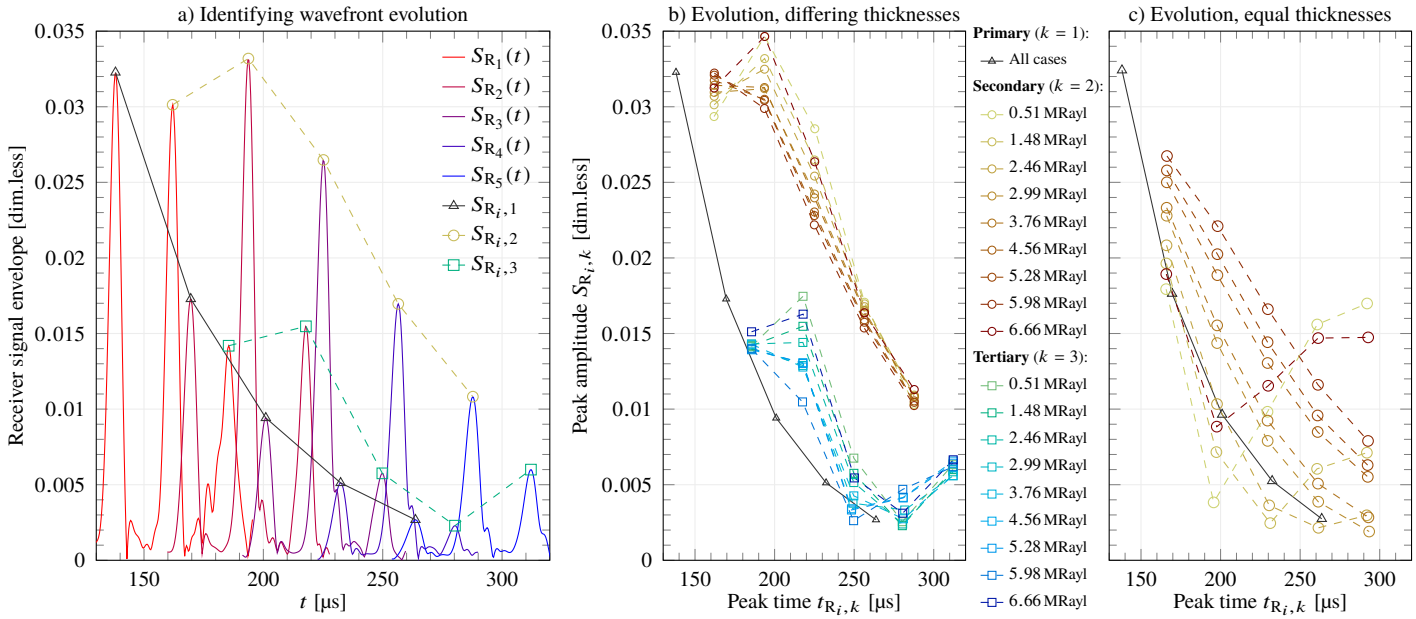

Figure 2: **a)** Envelopes of receiver signals $S_{\mathrm{R}_i}(t)$ for water (1.48 MRayl) in B-annulus, along with indicated evolution of primary, secondary, and tertiary wavefronts. **b)** Evolution of primary, secondary, and tertiary wavefronts for original casing thicknesses and 9 different B-annulus materials. **c)** Similarly, evolution of primary and secondary wavefronts for equal casing thicknesses.

original geometry in Figure 2b and in Figure 2c for a modified geometry with equally thick casings ($a_4 - a_3 = 0.408$ in) where the dispersion relations on both casings are very similar. For the original geometry there is a smaller effect of material variation on the secondary and tertiary wavefront, and the same evolution pattern is seen for all materials. For equal casing thicknesses the variation is much stronger on both the secondary and tertiary wavefronts. (To keep Figure 2c readable, the latter are not shown.) Generally, this matches earlier observations of the outer annulus impedance Z_{B} having a larger effect with equal casing thicknesses, which may come from the dispersion relations on the casings being more similar so that the wave packets on both casings tend to stay in phase [1]. Additionally, we see in both cases that the curves' behaviour is ordered by the B-annulus impedance with the exception of the highest-impedance material. The latter material behaves differently as its p-wave speed c_{p} is higher than the wave packet speed on the outer casing, which breaks the p-wave coupling [1, 3].

We define a logarithmic amplitude ratio, which for steady decay corresponds to attenuation in

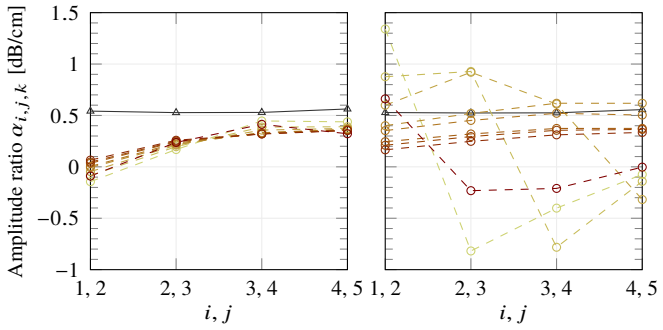

Figure 3: Amplitude ratios for primary and secondary wavefronts, using the same legend as the $S_{\mathrm{R}_i,k}$ plots in Figure 2. Left: Original casing thicknesses. Right: Equal casing thicknesses.

decibels per unit length, as

$$\alpha_{i,j,k} = \frac{20}{\Delta z_{i,j}} \log\left(\frac{S_{\mathrm{R}_i,k}}{S_{\mathrm{R}_j,k}}\right) \tag{1}$$

Here, $\Delta z_{i,j} = 10(j-i)$ cm is the distance between transducers R_i and R_j. Only $\alpha_{1,2,1}$ and $\alpha_{1,2,2}$ have previously been examined against Z_{B} as only two transducers have been available [1]. A plot of amplitude ratios for adjacent receivers R_i and $\mathrm{R}_j = \mathrm{R}_{i+1}$ is shown for both thickness cases in Figure 3. We see that the primary wavefronts are in constant steady decay, and in most cases we see that the secondary wavefronts have also settled into steady decay by the 4th or 5th receiver. A preliminary 10-receiver simulation for original casing thicknesses and water in the outer annulus suggested that the tertiary wavefront similarly settles into steady decay by the 7th or 8th receiver.

As we could expect from Figure 2b, the differences in amplitude ratio are not large for the original casing thicknesses. However, in this case we also found that all amplitude ratios are ordered by impedance, except for the highest-impedance material which diverges as explained above. For equal casing thicknesses, the three fluids and the highest-impedance material have not reached steady decay by the 5th receiver, but the attenuations are ordered by impedance for the other materials.

4. Possibility of inversion

We may use inversion to determine the properties of the system from measured wavefront amplitudes, given that we have a forward model where a set of wavefront amplitudes may be calculated from a given set of system parameters denoted as **a**. Several forward model alternatives are possible. Numerical simulations like those described in Section 2 are relatively straightforward,

but generally much too slow to be used for inversion. For this reason, faster semi-analytical forward models have been developed [2, 1], though the more general ones are by necessity very complex.

In this case we will apply a simple forward model designed to track the evolution of cascading Lamb wave packets on parallel casings separated by a fluid [1]. As we are now measuring the wave packet amplitudes indirectly through their emitted wavefronts, we will adapt the model accordingly. Several assumptions underlie this forward model, most notably that the dispersion relations on both casings are sufficiently similar that the wave packets on both casings approximately remain in the same relative phase. We will therefore only apply this model in the subset of simulated cases for which it is appropriate, namely for equal casing thicknesses and B-annulus materials with p-wave coupling to the casing. Even so, this model will still let us test the principle of determining the impedance Z_B from the five receivers' measured wavefront amplitudes $S_{\mathrm{R}_i,k}$.

The model follows the time evolution of the signed amplitude $B_n(t)$ of each wave packet n. $n = 1, 3, 5$ corresponds to the primary, secondary, and tertiary wave packet on the inner casing, respectively; it is these wave packets' amplitudes that we can measure indirectly through their emitted wavefronts impinging on the receivers. Even values of n correspond to wave packets on the outer casing, whose amplitudes cannot be measured by the receivers.

Each wave packet is attenuated as it leaks wavefronts into the adjacent media. The attenuation rate is characterised by the decay constants λ_I, λ_A, and λ_B, corresponding to the leakage into the interior, the A-annulus, and the B-annulus, respectively. For low impedances, these decay constants are proportional to the respective material impedances Z_I, Z_A, and Z_B [4]. The wavefronts' time of flight in the A-annulus between wave packets is denoted as Δt. When a wavefront in the A-annulus hits a casing, is is transmitted into the casing with a transmission coefficient T and reflected with a reflection coefficient R. Thus, the evolution of each wave packet's signed amplitude $B_n(t)$ can be expressed through the ordinary differential equation

$$\frac{dB_n(t)}{dt} = T\lambda_\mathrm{A} \sum_{i=1}^{n-1} R^{n-(i+1)} B_i[t-(n-i)\Delta t] - \lambda_n B_n(t), \quad \text{with} \quad \lambda_n = \begin{cases} \lambda_\mathrm{I} + \lambda_\mathrm{A} & \text{for } n \text{ odd,} \\ \lambda_\mathrm{A} + \lambda_\mathrm{B} & \text{for } n \text{ even.} \end{cases} \tag{2}$$

Here, λ_n is the total decay constant for wave packet n. The sum on the right-hand side corresponds to the total influence of earlier wave packets, while the second term corresponds to attenuation due

Table 2: Results of simulated annealing optimisation on the four lowest-impedance cases, with statistics based on 25 optimisation runs. The objective function from the set $\bar{\mathbf{a}}$ of mean parameters is also shown. Values of λ_B and $f(\bar{\mathbf{a}})$ are shown for additional cases in Figure 5.

Parameter	**0.51 MRayl** (fluid)	**1.48 MRayl** (fluid)	**2.46 MRayl** (fluid)	**2.99 MRayl** (solid)
$CB_1(0)$	0.514 ± 0.033	0.501 ± 0.027	0.451 ± 0.024	0.380 ± 0.030
t_0 [µs]	77.2 ± 4.1	71.9 ± 4.6	76.2 ± 2.7	67.3 ± 4.4
Δt [µs]	20.6 ± 0.8	20.5 ± 0.9	19.9 ± 0.7	21.2 ± 1.5
T	1.98 ± 0.03	1.83 ± 0.05	1.97 ± 0.03	1.87 ± 0.09
R	-0.98 ± 0.01	-0.97 ± 0.02	-0.98 ± 0.01	-0.99 ± 0.02
λ_w [ms^{-1}]	10.0 ± 0.2	9.9 ± 0.1	9.5 ± 0.2	9.0 ± 0.2
λ_B [ms^{-1}]	4.5 ± 0.5	10.0 ± 0.5	15.1 ± 0.3	19.4 ± 1.7
$f(\bar{\mathbf{a}})$	19.7×10^{-4}	12.4×10^{-4}	16.5×10^{-4}	33.0×10^{-4}

to leakage. Applying appropriate initial conditions for the first wave packet, we find

$$CB_1(t) = CB_1(0)\, \mathrm{e}^{-(\lambda_\mathrm{I}+\lambda_\mathrm{A})t} H(t - t_0), \tag{3}$$

where $B_1(0)$ is the primary wave packet's amplitude extrapolated back to $t = 0$, C is a constant conversion factor from the wave packet amplitude to the wavefront amplitude measurable by the receivers, t_0 is the wavefronts' time in flight in the interior from transmitter to casing and from casing to receiver, and H is the Heaviside function.

Some additional restrictions were imposed on the model parameters. In this through-tubing logging case with water in the interior and the A-annulus, we use a single decay constant for both, $\lambda_\mathrm{I} = \lambda_\mathrm{A} = \lambda_\mathrm{w}$. Additionally, stability considerations imply $T + R \leq 1$ and $T < 2$ [1]. No further restrictions were used, though in practice it might be possible to use prior knowledge to determine or limit some additional parameters.

To find optimised sets $\mathbf{a}$ of system parameters from the measured wavefront amplitudes $S_{\mathrm{R}_i,k}$, we used the stochastic optimisation method called simulated annealing. The objective function $f(\mathbf{a})$ was chosen as the L_2 norm of the deviation between modelled wavefront amplitudes and

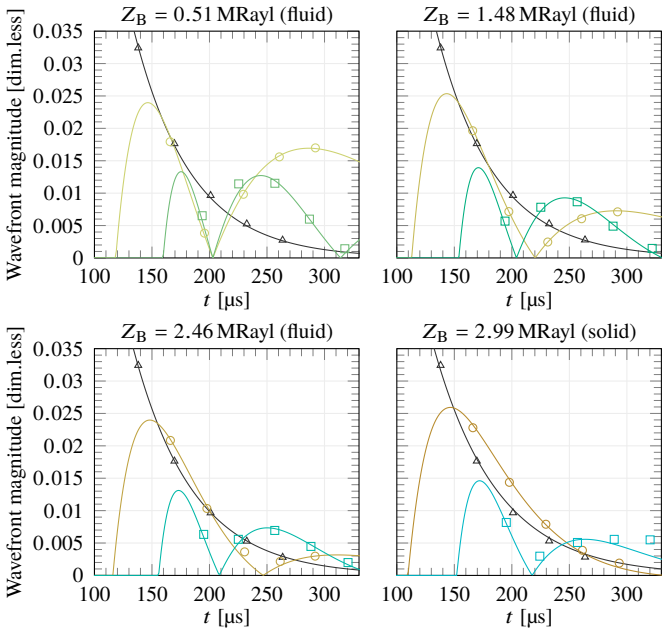

Figure 4: Optimised fits of simulated measurements $S_{\mathrm{R}_i,k}$ (marks) to modelled wavefront magnitudes $|CB_n(t)|$ (lines), using the sets $\bar{\mathbf{a}}$ of mean parameters from Table 2.

simulated measurements of these,

$$f(\mathbf{a}) = \sqrt{\sum_{i=1}^{5} \left[\left(|CB_1(t_{\mathrm{R}_i,1})| - S_{\mathrm{R}_i,1}\right)^2 + \left(|CB_3(t_{\mathrm{R}_i,2})| - S_{\mathrm{R}_i,2}\right)^2 + \left(|CB_5(t_{\mathrm{R}_i,3})| - S_{\mathrm{R}_i,3}\right)^2 \right]}, \quad (4)$$

with $B_n(t)$ determined from a parameter set $\mathbf{a}$. In other words, the model parameters were optimised to give a least-squares fit with the simulated measurements.

Due to the stochastic nature of simulated annealing, slightly different optimal parameter sets $\mathbf{a}$ are typically found from run to run. For this reason, Table 2 provides each resulting parameter for each of the four lowest-impedance cases as a mean value and a standard deviation, based on 25 well-converged runs. The start conditions for each case were chosen from preliminary runs; in all cases, the finally chosen start conditions fell within the determined standard deviation range. The fit between the measured wavefront peak amplitudes $S_{\mathrm{R}_i,k}$ and modelled wavefront magnitudes $|CB_n(t)|$ is shown in Figure 4.

From Table 2 and Figure 5 we find as expected that there is a near-linear correspondence between λ_{B} and Z_{B}, especially for low impedances where the underlying assumptions of the forward model are most valid. We can also find that there is a fairly large variation in t_0, even though there should not be as t_0 is physically determined by the constant geometry and material in the interior. Figure 4

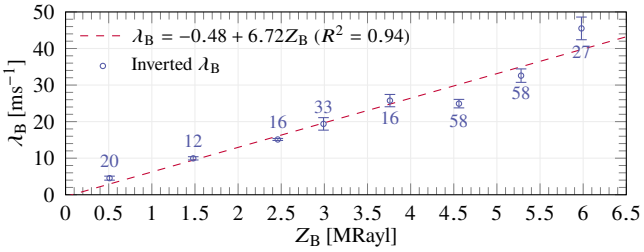

Figure 5: Linear fit of λ_B against Z_B for all but the highest-c_p material which, as explained above, lacks p-wave coupling to the Lamb wave; it therefore behaves differently to and cannot be compared to the other materials [1, 3]. Also shown for each λ_B are the objective function values $f(\bar{\mathbf{a}}) \times 10^4$, where lower values indicate more trustworthy results.

would suggest that the uncertainty in t_0 could be reduced by placing an additional receiver closer to the transducer to measure the rapid early evolution of the wavefronts; however, such measurements would be polluted by fluid-borne waves from the transmitter [1]. Similarly, there is a significant variation in T. In the fourth case, the higher value of $f(\bar{\mathbf{a}})$ indicates a significantly poorer fit between the simulated measurements and the model, suggesting that the model represents a poorer approximation for this higher-impedance material.

5. Conclusion

The wavefront amplitudes $S_{R_i,k}$ measured by the receivers in a pitch-catch setup are directly connected to the amplitude evolution of the leaky Lamb wave packets on the inner casing. This evolution depends on the system geometry and materials, including the impedance of the material bonded to the outer casing. With n receivers, we may thus measure n points along the evolution of each wave packet. Thus, with more receivers we can get a better picture of the wave packets' evolution and we can thus in principle determine the measured system's properties with greater accuracy. In this letter we have shown that using five receivers gives a clearer picture of the wave packet evolution than using two receivers [1].

Additionally, we were able to use a simple forward model to perform a limited inversion on a subset of simulated measurements, finding that the inverted model parameter λ_B varied nearly linearly with the impedance Z_B. To be able to perform a more general inversion, we would need to apply a more general forward model that can deal with factors such as differing dispersion relations on the casings, casing eccentricity, misaligned casings, and attenuating fluids. Still, our

findings indicate that the principle of determining the bonded material in the B-annulus from the measurements $S_{\mathrm{R}_i,k}$ is sound.

Acknowledgements

This work has been sponsored by Statoil. We acknowledge the aid of Statoil's Kevin Constable and Pål Hemmingsen.

References

[1] E. M. Viggen, T. F. Johansen, I.-A. Merciu, Simulation and modeling of ultrasonic pitch-catch through-tubing logging, Geophys. 81 (4) (2016) D369–D379. doi:10.1190/geo2015-0251.1.

[2] S. Zeroug, Analytical modeling for fast simulations of ultrasonic measurements on fluid-loaded layered elastic structures, IEEE Trans. Ultrason. Ferroelectr. & Freq. Control 47 (3) (2000) 565–574. doi:10.1109/58.842043.

[3] R. van Kuijk, S. Zeroug, B. Froelich, M. Allouche, S. Bose, D. Miller, J.-L. le Calvez, V. Schoepf, A. Pagnin, A novel ultrasonic cased-hole imager for enhanced cement evaluation, in: Internatl. Petro. Tech. Conf., 2005, p. 14. doi:10.2523/10546-MS.

[4] R. van Kuijk, J.-L. le Calvez, B. Froelich, Determination of the impedance of a material behind a casing combining two sets of ultrasonic measurements, U. S. Patent 7,149,146 B2 (2006).

[5] H. Wang, G. Tao, X. Shang, Understanding acoustic methods for cement bond logging, J. Acoust. Soc. Am. 139 (5) (2016) 2407–2416. doi:10.1121/1.4947511.

[6] J. P. Castagna, M. L. Batzle, R. L. Eastwood, Relationships between compressional-wave in elastic silicate rocks and shear-wave velocities, Geophys. 50 (4) (1985) 571–581. doi:10.1190/1.1441933.